Research Article

Journal of Molecular Recognition

Received: 6 May 2014, Revised: 20 August 2014, Accepted: 15 September 2014, Published online in Wiley Online Library

(wileyonlinelibrary.com) DOI: 10.1002/jmr.2434

On the molecular basis of the high affinity binding of basic amino acids to LAOBP, a periplasmic binding protein from *Salmonella typhimurium*

Nancy O. Pulido[a], Daniel-Adriano Silva[a,d†], Luis A. Tellez[a,e†], Gerardo Pérez-Hernández[b], Enrique García-Hernández[c], Alejandro Sosa-Peinado[a] and D. Alejandro Fernández-Velasco[a]*

The rational designing of binding abilities in proteins requires an understanding of the relationship between structure and thermodynamics. However, our knowledge of the molecular origin of high-affinity binding of ligands to proteins is still limited; such is the case for L-lysine–L-arginine–L-ornithine periplasmic binding protein (LAOBP), a periplasmic binding protein from *Salmonella typhimurium* that binds to L-arginine, L-lysine, and L-ornithine with nanomolar affinity and to L-histidine with micromolar affinity. Structural studies indicate that ligand binding induces a large conformational change in LAOBP. In this work, we studied the thermodynamics of L-histidine and L-arginine binding to LAOBP by isothermal titration calorimetry. For both ligands, the affinity is enthalpically driven, with a binding ΔCp of ~−300 cal mol^{-1} K^{-1}, most of which arises from the burial of protein nonpolar surfaces that accompanies the conformational change. Osmotic stress measurements revealed that several water molecules become sequestered upon complex formation. In addition, LAOBP prefers positively charged ligands in their side chain. An energetic analysis shows that the protein acquires a thermodynamically equivalent state with both ligands. The 1000-fold higher affinity of LAOBP for L-arginine as compared with L-histidine is mainly of enthalpic origin and can be ascribed to the formation of an extra pair of hydrogen bonds. Periplasmic binding proteins have evolved diverse energetic strategies for ligand recognition. STM4351, another arginine binding protein from *Salmonella*, shows an entropy-driven micromolar affinity toward L-arginine. In contrast, our data show that LAOBP achieves nanomolar affinity for the same ligand through enthalpy optimization. Copyright © 2015 John Wiley & Sons, Ltd.
Additional supporting information may be found in the online version of this article at the publisher's web site.

Keywords: structural thermodynamics; isothermal titration calorimetry; ligand recognition; enthalpy-driven binding; Venus flytrap mechanism

A quantitative correlation between structure and thermodynamics is crucial for the understanding of the molecular basis that endows proteins with the ability to recognize ligands with high affinity and selectivity, as well as for addressing the problem of rational ligand design (Whiteside and Krishnamurthy, 2005). While there is abundant information about the structures of proteins bound to small ligands, binding thermodynamic parameters are still scarce for many of those systems. This is the case of substrate binding proteins (SBPs), a large and diverse group of proteins that comprises families such as ATP-binding cassette (ABC) transporters, regulatory systems, ligand-gated ion

* *Correspondence to: D. Alejandro Fernández-Velasco, Laboratorio de Fisicoquímica e Ingeniería de Proteínas, Facultad de Medicina, Universidad Nacional Autónoma de México, Circuito Exterior, Ciudad Universitaria, México 04510, DF, México.*
E-mail: fdaniel@unam.mx

† *These authors contributed equally to this work.*

a *N. O. Pulido, D.-A. Silva, L. A. Tellez, A. Sosa-Peinado, D. A. Fernández-Velasco*
Laboratorio de Fisicoquímica e Ingeniería de Proteínas, Departamento de Bioquímica, Facultad de Medicina, Universidad Nacional Autónoma de México, México, DF, Mexico

b *G. Pérez-Hernández*
Departamento de Ciencias Naturales, Universidad Autónoma Metropolitana-Cuajimalpa, México, DF, Mexico

c *E. García-Hernández*
Instituto de Química, Universidad Nacional Autónoma de México, Circuito Exterior, Ciudad Universitaria, México 04510, DF, Mexico

d *D.-A. Silva*
Biochemistry Department, University of Washington, Seattle, WA, USA

e *L. A. Tellez*
Department of Psychiatry, Yale University School of Medicine, New Haven, CT, USA

Abbreviations: *PBP, periplasmic binding protein; SBP, substrate binding protein; ITC, isothermal titration calorimetry; LAOBP, L-lysine–L-arginine–L-ornithine PBP; His, L-histidine; Arg, L-arginine; Lys, L-lysineΔH_b, binding enthalpy; ΔS_b, binding entropy; ΔG_b, Gibbs binding free energy; ΔCp_b, binding heat capacity; K_b, equilibrium binding constant; K_d, dissociation constant; ΔH_{int}, intrinsic binding enthalpy; ΔH_{dsolv}, desolvation enthalpy; ΔS_{conf}, ΔS_{dsolv}, and ΔS_{r-t}, conformational, desolvation and roto-translational entropy changes, respectively; ΔA_i, surface area change for surface area of the type i; ΔH_{ion}, ionization enthalpy; ΔCp_{dsol}, desolvation heat capacity change.*

Journal of Molecular Recognition

channels, transcriptional regulators, and G-protein-coupled receptors (Felder *et al*., 1999; De Wolf and Brett, 2000; Dwyer and Hellinga, 2004; Berntsson *et al*., 2010). There are hundreds of known SBPs, with more than 120 unique entries deposited in the Protein Data Bank (PDB). Although SBPs share little sequence identity, all of them are topologically related in their two lobes, connected by a hinge region (Felder *et al*., 1999). The functionally relevant signature of SBPs is in the realm of conformational dynamics. SBPs display the so-called Venus flytrap mechanism, a large-scale rigid body reorientation of the lobes usually triggered by the binding event, which leads a conformational change where the ligand becomes completely buried in a cleft between the lobes (Felder *et al*., 1999; De Wolf and Brett, 2000; Dwyer and Hellinga, 2004).

Periplasmic binding proteins (PBPs) are the founding family of the SBP superfamily (Ames, 1986; Quiocho, 1990). Originally described in the ABC transport system of Gram-negative bacteria, PBPs are required for chemotaxis and for the transport of a wide variety of low-molecular-weight metabolites (Ames, 1986). PBPs have been used for the design of nanosensors that couple a change in fluorescence with the closure event, thereby straightforwardly detecting metabolites and ions (Vercillo *et al*., 2007; Jeffery, 2011). The PBP scaffold is very promising for the design of new binding abilities (Dwyer and Hellinga, 2004); however, the limited success obtained so far has reopened the discussion of whether computational protein design is still an unsolved problem that needs reconsideration in its details (Schreier *et al*., 2009).

L-Lysine (Lys)–L-arginine (Arg)–L-ornithine PBP (LAOBP), the Lys, Arg, and L-ornithine binding protein of *Salmonella typhimurium*, is composed of two lobes (lobe I, residues 1–88 and 195–238; lobe II, residues 93–185), connected by a hinge region composed of two short peptide segments (Oh *et al*., 1993). The crystal structures of LAOBP in unligated and ligand-bound forms have been reported (Oh *et al*., 1993, 1994). In the absence of the ligand, the protein shows an open conformation, with the two lobes separated from each other. In contrast, when bound to Lys, Arg, or L-histidine (His), LAOBP adopts a closed conformation, with the two lobes considerably rotated in relation to the extended conformation (~50°). Equilibrium dialysis experiments have shown that LAOBP binds Arg, Lys, and L-ornithine with low nanomolar affinity (Nikaido and Ames, 1992), that is, within the highest affinities reported for PBPs. On the other hand, LAOBP binds to His with an affinity similar to that displayed by many other PBPs (Nikaido and Ames, 1992). Thus, LAOBP is an excellent model to study the factors that modulate high-affinity binding. In what follows, we present a study of LAOBP binding to Arg and His by isothermal titration calorimetry (ITC). The role of water molecules and proton uptake in ligand binding were experimentally evaluated. The data were then interpreted in terms of structural information to gain insights on the molecular origin of the high-affinity binding of basic amino acids to LAOBP. Finally, the data obtained were compared with those reported for other PBPs

EXPERIMENTAL PROCEDURES

Expression and purification of LAOBP

E. coli strain BL21-AI was transformed with the pET12-LAOBP plasmid carrying the *argT* gene, and the expression was induced with 0.25% L-arabinose for 4 h. Cells were harvested by centrifugation (5000 rpm for 15 min), resuspended in potassium acetate (KOAc) 10 mM (pH 5.1), 20% sucrose, and 1 mM EDTA. The periplasmic fraction was collected by the osmotic shock using KOAc 10 mM (pH 5.1). After centrifugation (11 000 rpm for 20 min), in order to eliminate bound amino acids, the protein was dialyzed for several times against 2 M guanidinium chloride (GdnHCl) and bis-tris propane 5 mM (pH 8.5). GdnHCl was then removed by concentration and dilution with 40 ml of bis-tris propane, 5 mM (pH 8.5). The sample was finally applied to an anionic exchange Source Q column and eluted using a 0–250-mM lineal NaCl gradient. LAOBP was eluted near 50 mM NaCl. A single band with purity higher than 98% was observed in sodium dodecyl sulfate PAGE.

ITC experiments were performed at pH 8.0 in a 0.01-M 4-(2-hydroxyethyl)-1-piperazineethanesulfonic acid (HEPES) buffer solution. This pH value was chosen because from unfolding experiments in urea, we have determined that the maximal stability of LAOBP is observed at this pH (Vergara R, et. al. in preparation). We noted some artifacts in the calorimetric measurements when LAOBP was processed using regenerated cellulose dialysis membranes (data not shown); therefore, buffer was exchanged using an Amicon Ultra-4 centrifugal filter device (MW cutoff 10 000). After degassing the samples, protein concentration was determined spectrophotometrically, using an extinction coefficient of 26 025 M^{-1} cm^{-1} at 280 nm. Ligand solutions were prepared by dissolving amino acids in the buffer previously equilibrated with the protein solution. Unless otherwise specified, all chemical reagents were from Sigma Chemical Co.

ITC

ITC experiments were performed using the high-precision MicroCal™ iTC_{200} System (GE Healthcare, Northampton, MA, USA). Binding of LAOBP to His and Arg was measured in the temperature range of 15 to 40°C. LAOBP concentration was typically 0.03–0.07 mM, while ligand concentration in the syringe was 1.1–1.6 mM. The dilution heat of the ligand was obtained via addition of the ligand to a buffer solution under identical conditions and injection schedule used with the protein sample. The binding constant (K_b), the enthalpy change (ΔH_b), and the stoichiometry (n) were determined by nonlinear fitting of normalized titration data using a model of identical and independent binding sites (Wiseman *et al*., 1989). Titrations of LAOBP with Arg were carried out using a displacement protocol, which consists of adding a weak competitive ligand (His, in this case) to the protein solution in the calorimetric cell in order to artificially lower the affinity of the high-affinity ligand (Arg). The binding equations for these assays have been reported by Velázquez-Campoy and Freire (2006).

Changes in solvent-accessible surface areas

Accessible surface areas were calculated using the NACCESS program (Hubbard, S.J. and Thornton, J.M. (1993) NACCESS, Department of Biochemistry and Molecular Biology, University College, London), using a probe radius of 1.4 Å and slice width of 0.1 Å. 3D coordinates for apo LAOBP and complexed to His and Arg were extracted from PDB files 2LAO, 1LAG, and 1LAF, respectively (Oh *et al*., 1994). Carbon and sulfur atoms contribute to apolar surface (A_{ap}), whereas oxygen and nitrogen atoms add to polar surface (A_p). Changes in solvent-accessible surface area of type i (ΔA_i) were estimated from the difference between the

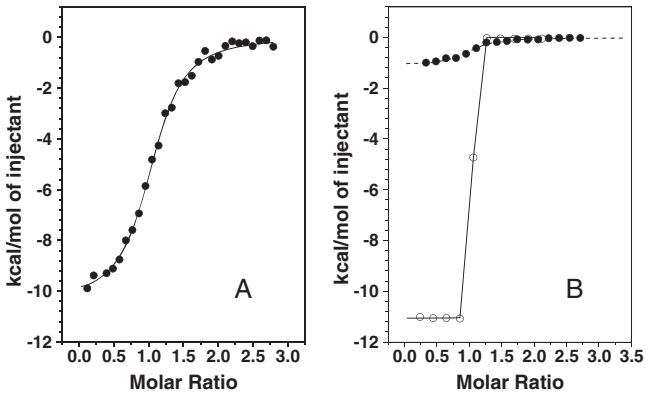

Figure 1. Representative ITC profiles for ligand binding to LAOBP at 25°C, in 10 mM HEPES, pH 8.0. (A) LAOBP (0.05 mM) titrated with His (1.6 mM). (B) Solid circles correspond to a displacement experiment with LAOBP (0.05 mM) preincubated with His (2 mM), which was titrated with Arg (1.8 mM). Open circles correspond to a direct titration of LAOBP (0.07 mM) with Arg (2 mM).

complex and the sum of the unbound state and the ligand. Two different calculations were performed to represent the unbound state: in the first (ΔA^O), the crystal structure of the "open" form was used, whereas in the second (ΔA^C), the coordinates of the closed conformation with the ligand removed were used.

ΔA-based calculations of ΔCp

To estimate ΔCp from structural data, we used the semiempirical relationship obtained from protein folding data (Makhatadze and Privalov, 1995):

$$\Delta Cp_{calc} = -0.21\Delta A_p + 0.51\Delta A_{ap} \quad (1)$$

where coefficient units are cal mol^{-1} K^{-1} Å^{-2}.

RESULTS

Thermodynamics of His and Arg binding to LAOBP

Early measurements showed that LAOBP binds to His and to Arg in the low μM and low nM range, respectively (Nikaido and Ames, 1992). Consistent with that, we were able to solve the calorimetric binding parameters for His through direct titration experiments, while for Arg, it was necessary to carry out displacement experiments using His as competitive ligand. Figure 1 shows representative binding isotherms for LAOBP interaction with the two amino acids. Table 1 summarizes calorimetric results obtained as a function of temperature after correction for protonation effects (*vide infra*). For both complexes, the average experimental stoichiometry was 0.99 ± 0.01. Binding of the two ligands was enthalpically driven throughout the temperature range spanned (Table 1, Figure 2). The entropy change was favorable at 15°C and unfavorable at the higher temperatures, indicating that both complexes reach maximum stability at around room temperature. Arg exhibited a more favorable enthalpy than His, an excess that increased with temperature. In contrast, the difference in entropy between the two complexes vanished at 40°C. As a consequence, the affinity of Arg relative to His was 3800-fold at 15°C and decreases to 300-fold at 40°C. Assuming linear dependence on temperature, regression analysis of enthalpy data yielded ΔCp_b values of −264 ± 41 for His and −299 ± 41 cal mol^{-1} K^{-1} for Arg. Similar results were obtained from the analysis of entropy data (−267 ± 47 for His and −320 ± 51 cal mol^{-1} K^{-1} for Arg).

Dissociation constants for LAOBP complexed with His (K_d = 0.5 μM) and Arg (K_d = 14 nM) had previously been obtained from equilibrium dialysis experiments carried out at 4°C, pH 7.0 (Nikaido and Ames, 1992). Extrapolation of our ITC data to 4°C (pH 8.0) yields somewhat different K_d values: 1.4 μM for His and 0.3 nM for Arg. We have no explanation for these differences; however, it should be noted that this comparison involves an extrapolation, changes in experimental conditions (temperature, pH, and buffer), and different measurement techniques.

Coupled equilibria

LAOBP's ligand binding was assessed to unveil the possible existence of coupled equilibria (Pulido *et al*., 2008). Proton exchange was evaluated by performing calorimetric titrations using buffers of different ionization enthalpy (ΔH_{ion}). Depending on the number of protons exchanged (ν), the measured enthalpy (ΔH_{obs}) varies according to (Baker and Murphy, 1998):

$$\Delta H_{obs} = \nu\Delta H_{ion} + \Delta H_0 \quad (2)$$

where ΔH_0 is the binding enthalpy corrected for buffer protonation effects. For His binding, a marked dependence of ΔH_{obs}

Table 1. Thermodynamic parameters for the binding of His and Arg to LAOBP

Complex	Temperature (°C)	K_d (nM)	ΔG_b (kcal mol^{-1})	ΔH_b (kcal mol^{-1})[a]	$T\Delta S_b$ (kcal mol^{-1})
LAOBP–His	15	1900 ± 130	−7.5	−7.0 ± 0.2[d]	+0.5
	25	2700 ± 190	−7.6	−8.2 ± 0.2[d]	−0.6
	30	2900 ± 145	−7.7	−9.6 ± 0.1[d]	−1.9
	35	4500 ± 270	−7.5	−12.1 ± 0.1[d]	−4.6
	40	6900 ± 450	−7.4	−13.3 ± 0.3[d]	−5.9
LAOBP–Arg	15	0.50 ± 0.05	−12.1	−9.7 ± 0.02	+2.4
	25	0.96 ± 0.01	−12.3	−11.3 ± 0.1	+1.0
	30	2.90 ± 0.4	−11.8	−12.8 ± 0.1	−1.1
	35	8.80 ± 1.0	−11.4	−15.5 ± 0.2	−4.1
	40	22 ± 4.0	−11.0	−16.9 ± 0.1	−5.9

[a]Enthalpy changes for His binding were corrected for protonation effects as follows: 4.9 kcal mol^{-1} was substracted because of deprotonation of the HEPES buffer, and 7.0 kcal mol^{-1} was added to account for the protonation of His. Data for buffer ionization enthalpies as a function of temperature were taken from Goldberg *et al*. (2002).

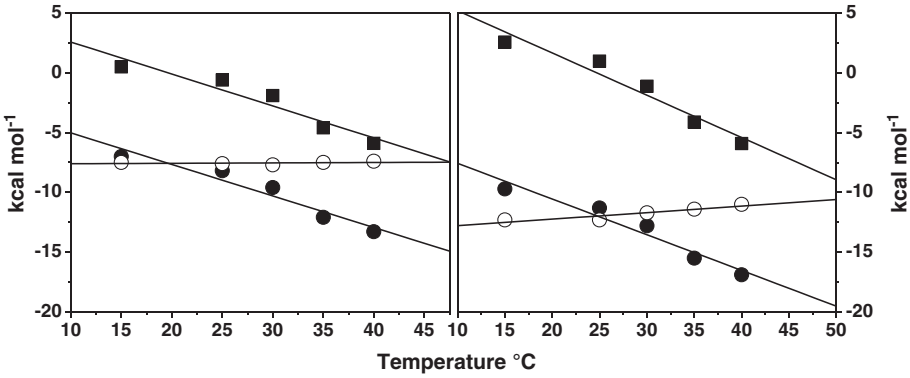

Figure 2. Thermal dependence of ΔH (black circle), $T\Delta S$ (black square), and ΔG (white circle) for the interaction of LAOBP with His (A) and Arg (B), in 10 mM HEPES, pH 8.0. ΔCp_b values, calculated from the least squares linear fitting of enthalpy data versus temperature, were -264 ± 41 and -299 ± 41 cal mol^{-1} K^{-1} for His and Arg, respectively.

on the buffer used was observed (Figure 3A), a behavior consistent with the net uptake of 1.02 ± 0.4 protons. Because ΔH_{obs} can be measured accurately from rectangular-shaped isotherms (Figure 1B), direct titrations of LAOBP with Arg were carried out in order to measure proton exchange effects. For this last ligand, ΔH_{obs} was almost independent of the buffer used (± 0.1 kcal mol^{-1}). This result reveals that His, which has neutral charge at the experimental conditions used ($pK_a = 6.0$), protonates upon binding. Accordingly, the ionization enthalpies of HEPES and His (Goldberg *et al*., 2002) were respectively added to and subtracted from the calorimetric data to obtain binding parameters free of both buffer and ligand protonation contributions (refer to footnote to Table 1). In fact, molecular dynamics simulations predicted that because of its contribution to stacking interaction with aromatic residues in the binding site, only the protonated His tautomer binds to LAOBP (Silva *et al*., 2011). These findings explain the broader optimal pH for Arg binding as compared with a narrower and acid-shifted binding for His (Nikaido and Ames, 1992).

The number of counterions exchanged upon binding (ΔN_{Cl}) was determined from the dependence of K_b on the solution ionic strength (I) (Record *et al*., 1998):

$$\Delta N_{Cl} = \frac{\partial \log K_b}{\partial \log I} \tag{3}$$

Figure 3B shows that His binding was almost independent of NaCl concentration in the 0.02–0.3-M range, indicating the release of 0.2 ± 0.0 counterions upon binding.

Finally, the number of structural water molecules exchanged upon complex formation (ΔN_W) was estimated by performing measurements at varying sucrose concentrations (Parsegian *et al*., 1995). According to the osmotic stress theory, ΔN_W determines the dependence of K_b on the solution osmolality ([osmol]):

$$\Delta N_W = -55.6 \frac{\delta \ln K_b}{\delta [osmol]} \tag{4}$$

As shown in Figure 3C, K_b for His decreases with an increase in sucrose concentrations, revealing that 3 ± 1 water molecules are sequestered upon binding of this amino acid. This result is coincident with the crystal structure of the LAOBP–His complex, where three water molecules were observed in the binding site (Figure 4A). Unfortunately, we did not succeed in determining proton and water molecule exchanges for Arg. Competitive calorimetric traces in the presence of high salt or osmolyte concentrations were too noisy, precluding a reliable estimation of K_b variation. Nevertheless, inspection of the LAOBP–Arg structure reveals the presence of four structural water molecules at

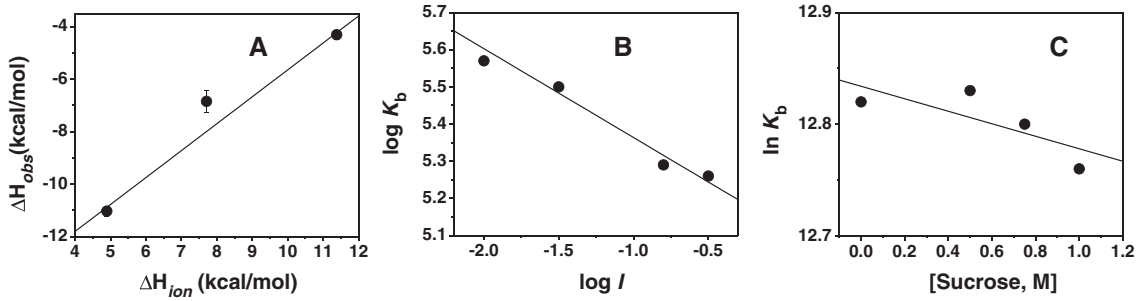

Figure 3. Coupled equilibria to the formation of the LAOBP–His complex. (A) Proton exchange determined from ITC titrations carried out in HEPES, $\Delta H_{ion} = 4.9$ kcal mol^{-1}; 2-[[1,3-dihydroxy-2-(hydroxymethyl)propan-2-yl]amino]ethanesulfonic acid, $\Delta H_{ion} = 7.7$ kcal mol^{-1}, and TRIS, $\Delta H_{ion} = 11.3$ kcal mol^{-1}. The data fit to Eqn 3 indicate that 1.02 ± 0.4 protons are taken. (B) Counterion exchange. Binding experiments at different ionic strength (I) were carried out with different NaCl concentrations. Data fit to Eqn 4 show that 0.24 ± 0.03 counterions are incorporated upon complex formation. (C) Osmotic stress measurements were performed using sucrose as the osmolyte. Data fit to Eqn 5 indicate that 3 ± 1 water molecules are sequestered upon binding. Data represent the average of three independent measurements.

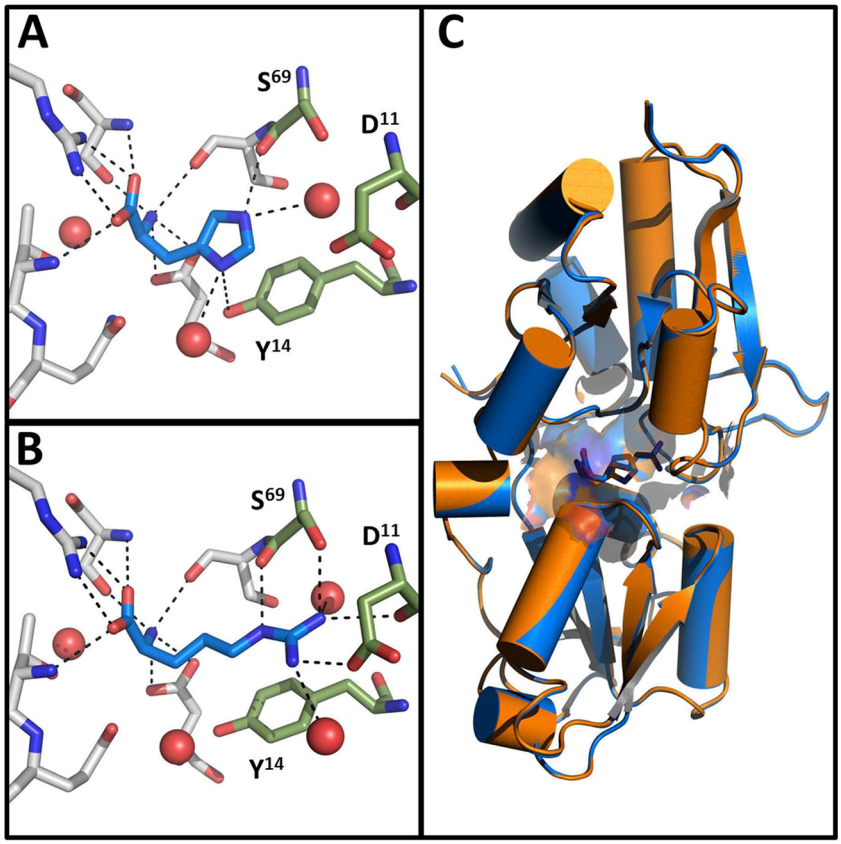

Figure 4. Schematic representations of the X-ray structures of LAOBP–His (PDB code 1LAG) and LAOBP–Arg (PDB code 1LAF) complexes (Oh *et al*., 1994). Details of the protein's binding site occupied by His and Arg are shown in panels (A) and (B), respectively. Hydrogen bonds are represented in dashed lines. Crystallographic water molecules are shown as spheres. The overlapping of protein conformations in the two complexes is shown in panel (C). The root-mean-square deviation (over Cα atoms) between the two protein structures is 0.2 Å. It can be seen that the two ligands are completely buried in the protein's binding site.

the binding site, three of which occupy equivalent positions to those observed in the LAOBP–His complex (Figure 4B). Thus, it seems reasonable to assume that Arg and His bindings are accompanied by the uptake of a similar number of structural water molecules.

DISCUSSION

Crystallographic structures (Oh *et al*., 1994) revealed that LAOBP adopts essentially the same conformation when bound to His and Arg (Figure 4C). In both complexes, the ligands are completely buried at the binding site with all potential hydrogen-bonding donors and acceptors fully coordinated. Overall, the main differences between the complexes are restricted to the polar interactions formed by the protein and the side chain of the ligand. As illustrated in Figure 4A–B, while the guanidinium group forms four direct hydrogen bonds with the protein, the imidazolium group forms only two direct hydrogen bonds. The two additional hydrogen bonds made by Arg, established with Asp^{11}, have been proposed to be mainly responsible for the differences in binding energy between the two complexes (Oh *et al*., 1994). Here, we found that at 25°C, Arg binding to LAOBP is -4.7 kcal mol^{-1} more stable than His binding (Table 1). In order to understand the determinants of this difference, we present a structural–energetic analysis that involves the full set of thermodynamic functions determined herein.

Table 2. Surface area changes and structure-based estimations of ΔCp for the formation of LAOBP complexes[a,b]

Complex	ΔA_p^C	ΔA_{ap}^C	ΔA_p^O	ΔA_{ap}^O	ΔCp_{calc}^C	ΔCp_{calc}^O	ΔCp_{exp}
LAOBP–His	−206	−173	−300	−565	−72	−252	−264
LAOBP–Arg	−275	−160	−371	−643	−60	−286	−299

[a]The atomic coordinates for the open conformation and the closed conformations bound to His and Arg were taken from the PDB files 2LAO, 1LAG, and 1LAF, respectively.
[b]ΔA and ΔCp values were calculated taking the free protein as either in the open (superscript O) or in the closed (superscript C) conformation. ΔCp_{calc} values for His and Arg include contributions from the freezing of three and four structural water molecules, respectively, using a change of -9 cal mol^{-1} K^{-1} per molecule (Bello *et al*., 2008).

Journal of Molecular Recognition

Heat capacity changes

Heat capacity changes for ligand binding and protein folding have been correlated with changes in solvent exposition of polar (ΔA_p) and apolar surfaces (ΔA_{ap}; Sturtevant, 1977; Murphy and Freire, 1992; Spolar *et al*., 1992; Myers *et al*., 1995; Cooper, 2005; Prabhu and Sharp, 2005; Chavelas and García-Hernández, 2009).Table 2 lists the area changes for the two LAOBP complexes studied herein, as determined from crystal structures. Two different calculations were performed: one in which the whole conformational change was modeled using the open conformation for the unbound state (ΔA^O) and another in which the free protein was supposed to be prefrozen in the closed conformation (ΔA^C), that is, assuming a rigid-body-like association. Using these area changes and the parameterization reported by Makhatadze and Privalov (1995), corresponding ΔCp values were estimated for ligand binding coupled $\left(\Delta Cp^O_{calc}\right)$ or not $\left(\Delta Cp^C_{calc}\right)$ to the protein conformational change. ΔCp_{calc} values listed in Table 2 include the contribution of three or four sequestered water molecules to the complexes of LAOBP with His or Arg, respectively, considering a contribution of -9 cal mol^{-1} K^{-1} by a water molecule (Bello *et al*., 2008). Clearly, ΔCp^O_{calc} values satisfactorily reproduce the experimental values, while ΔCp^C_{calc} values are significantly less negative. These results lend thermodynamic support to the structural picture that upon ligand binding, LAOBP undergoes a large conformational change, that is, in the absence of a ligand, the protein mostly populates the open state (Nikaido and Ames, 1992; Oh *et al*., 1994). Although it is commonly considered that this behavior is characteristic of PBPs, recent studies indicate that not necessarily all members fully undergo the "Venus flytrap" change. In some cases, the apoprotein can also visit the closed conformation with considerable frequency (Chu *et al*., 2014).

The heat capacity changes observed for the binding of His and Arg to LAOBP (Table 2) are more negative than those observed for the rigid-body binding of small molecules to proteins (~5 to -100 cal mol^{-1} K^{-1}; García-Hernández *et al*., 2003; Zakariassen and Sørlie, 2007; Zakariassen *et al*., 2008; Chu *et al*., 2014). In contrast, the ΔCp_b values determined in this work, as well as the few values reported for PBPs in the literature, are large and negative: -376 and -436 cal mol^{-1} K^{-1} for the complexes of L-galactose and L-arabinose with the arabinose binding protein (Fukada *et al*., 1983) and -207 cal mol^{-1} K^{-1} for the binding of maltose to the maltose binding protein (Thomson *et al*., 1998).

ΔCp_b can be also partitioned into protein ($\Delta Cp_{dsol,P}$) and ligand desolvation terms ($\Delta Cp_{dsol,L}$). Because the ligands are completely buried in the binding site, $\Delta\Delta Cp_{dsol,L}$ can be calculated directly from differences in the overall solvation heat capacities of the

Table 3. Structural energetics of LAOBP complexes at 25°C[a,b]

Ligand	ΔCp_b	$\Delta Cp_{dsol,}$[b]	$T\Delta S_b$	$T\Delta S_{dsol,L}$	$T\Delta S_{conf,L}$	ΔH_b	$\Delta H_{dsol,L}$	ΔH_{int}	ΔG_b
Arg	−299	−40	1.0	7.3	−1.9	−11.3	23.8	$-35.1-\Delta H_{\boldsymbol{dsol,P}}$	−12.3
His	−264	−18	−0.6	5.3	−1.0	−8.2	16.6	$-24.8-\Delta H_{\boldsymbol{dsol,P}}$	−7.6
ΔΔX[c]	−35	−22	1.6	2.0	−0.9	−3.1	7.2	−10.3[d]	−4.7

[a]ΔH, ΔG, and $T\Delta S$ in kcal mol^{-1}; ΔCp in cal mol^{-1} K^{-1}.
[b]Desolvation magnitudes for His and Arg were taken from references (Makhatadze and Privalov, 1990, 1993a; Doig and Sternberg, 1995; Thomson *et al*., 1998).
[c]$\Delta\Delta X = \Delta X_{Arg} - \Delta X_{His}$ where $\Delta X = \Delta G$, ΔH, $T\Delta S$, or ΔCp.
[d]Assuming $\Delta\Delta H_{\boldsymbol{dsol,P}} = 0$.

Table 4. Thermodynamic binding signatures of selected PBPs

Protein[a]	Source	Ligand	K_d	ΔG (kcal mol^{-1})	ΔH (kcal mol^{-1})	$T\Delta S$ (kcal mol^{-1})	T(°C)/pH	Reference
WtpA	*Pyrococcus furiosus*	Tungstate	17.0 pM	−14.7	5.3	20.0	25/8.0	[b]
HmuT	*Yersinia pestis*	Heme group	0.3 nM	−13.1	−2.1	11.0	30/7.5	[c]
LAOBP	*Salmonella thypimurium*	Arginine	1.0 nM	−12.3	−11.3	1.0	25/8.0	This work
PotF	*E. coli*	Putrescine	4.8 nM	−11.6	−26.0	−14.4	22/8.0	[d]
OppA	*E. coli*	Nle	9.5 nM	−11.0	4.7	15.7	25/7.0	[e]
STM4351	*Salmonella enterica*	Arginine	2.9 μM	−7.5	1.4	8.9	25/7.2	[f]
TogB	*Yersinia enterocolitica*	UnsatdigalUA	5.3 μM	−7.1	−18.5	−11.4	25/8.0	[g]

[a]WtpA, tungsten transport protein A; HmuT, periplasmic heme binding protein; PotF, polyamine binding protein F; OppA, oligopeptide binding protein; STM4351, serovar typhimurium periplasmic binding protein; TogB, oligogalactouronide binding protein.
[b]Bevers *et al*., 2006.
[c]Mattle *et al*., 2010.
[d]Scheib *et al*., 2014.
[e]Sleigh *et al*., 1999.
[f]Stamp *et al*., 2011.
[g]Abbott & Boraston 2007.

two amino acids (Table 3). According to data reported by Makhatadze and Privalov (1990), $\Delta\Delta Cp_{dsol,L}$ (Arg minus His) is -22 cal mol^{-1} K^{-1}, a value that is very similar to the calorimetric $\Delta\Delta Cp_b$ (-35 cal mol^{-1} K^{-1}, Table 3). This result clearly shows that, within experimental error, $\Delta\Delta Cp_{dsol,P}$ is close to zero. In other words, the analysis indicates that protein solvation changes upon Arg or His binding are thermodynamically equivalent.

Enthalpy and entropy changes

The binding entropy ($T\Delta S_b$) can be described in terms of the sum of five major contributions, namely, the protein and the ligand conformational changes, $T\Delta S_{conf,P}$ and $T\Delta S_{conf,L}$, respectively, the desolvation changes, $T\Delta S_{dsol,P}$ and $T\Delta S_{dsol,L}$, and the roto-translational contribution, $T\Delta S_{r\text{-}t}$. For the difference in the entropy of both ligands, we have

$$\Delta(T\Delta S_b) = \Delta\left(T\Delta S_{conf,L}\right) + \Delta\left(T\Delta S_{dsol,L}\right) + \Delta\left(T\Delta S_{conf,P}\right) + \Delta\left(T\Delta S_{dsol,P}\right) + \Delta\left(T\Delta S_{r-t}\right) \quad (5)$$

Because the same number of rota-translational degrees of freedom is lost in two complexes, $\Delta(T\Delta S_{r\text{-}t}) = 0$. On the other hand, overall desolvation and conformational entropy of Arg and His have been experimentally determined (Makhatadze and Privalov, 1990, 1993a). Being a bulkier amino acid with more rotatable bonds, upon complete sequestration from solvent, Arg yields more favorable dehydration entropy values and more unfavorable conformational entropy values in relation to His (Table 3). Using these data, $\Delta(T\Delta S_b)$ (Arg minus His) is estimated as 1.1 kcal mol^{-1}. This magnitude is very close to that obtained from the experimental $\Delta T\Delta S_b$ (=1.6 kcal mol^{-1}, Table 3), a result that is consistent with the picture that the protein's solvation and conformational changes upon Arg or His binding are equivalent, that is, $\Delta(T\Delta S_{dsol,P}) \approx \Delta(T\Delta S_{conf,P}) \approx 0$.

Finally, the binding enthalpy is a measure of the interaction strength between molecular partners (ΔH_{int}) relative to the energy penalty paid by desolvation of the protein and the ligand's contact surfaces ($\Delta H_{dsol,P}$, and $\Delta H_{dsol,L}$, respectively). Therefore, the enthalpy difference between the two ligands ($\Delta\Delta H_b$) is expressed as

$$\Delta\Delta H_b = \Delta\Delta H_{int} + \Delta\Delta H_{dsol,L} + \Delta\Delta H_{dsol,P} \quad (6)$$

$\Delta H_{dsol,L}$ values for Arg and His, taken from Makhatadze and Privalov (1993a), are shown in Table 3. According to these data, $\Delta\Delta H_{dsol,L}$ (Arg minus His) amounts to 7.2 kcal mol^{-1}. Because $\Delta\Delta H_{dsol,P}$ can be assumed to be zero, the difference in the intrinsic interaction between the two ligands ($\Delta\Delta H_{int}$) is -10.3 kcal mol^{-1} (Table 3). As the main difference in the interactions of LAOBP with its two ligands seems to be the two extra hydrogen bonds formed with Arg (Figure 4A–B), it follows that the formation of each hydrogen bond liberates, on the average, -5.1 kcal mol^{-1} of enthalpy. This calculation is in agreement with enthalpy changes for the formation of hydrogen bonds in the vapor phase (Rose and Wolfenden, 1993; Makhatadze and Privalov, 1993b; Lazaridis *et al.*, 1995).

Diversity in binding signatures of PBPs

Table 4 collects ligand-binding data for selected PBPs that have been characterized calorimetrically (a comprehensive compilation of ITC data is presented in Table S1). Clearly, the thermodynamic signatures observed in the PBP family are widely diverse (Davies *et al.*, 1999; Sleigh *et al.*, 1999; Cadieux *et al.*, 2002; Bevers *et al.*, 2006; Abbott and Boraston, 2007; Prajapati *et al.*, 2007; Zhang *et al.*, 2007; Schreier *et al.*, 2009; Mattle *et al.*, 2010; Stamp *et al.*, 2011; Aryal *et al.*, 2012; Ortega *et al.*, 2012; Hu *et al.*, 2013; Salmon *et al.*, 2013; Scheib *et al.*, 2014). Tungsten transport protein A and periplasmic heme binding protein show the largest affinities; for both proteins, picomolar affinity is achieved on the basis of a largely favorable entropy change. LAOBP, polyamine binding protein F (PotF) and oligopeptide binding protein (OppA) all exhibit low nanomolar affinity. In relation to LAOBP, PotF shows a much more negative enthalpy, which, in turn, is offset by also much more unfavorable binding entropy. On the contrary, OppA binding is entropically driven. Finally, serovar typhimurium PBP (STM4351) and oligogalactouronide binding protein exemplify micromolar-affinity PBP members with opposing enthalpic and entropic behaviors.

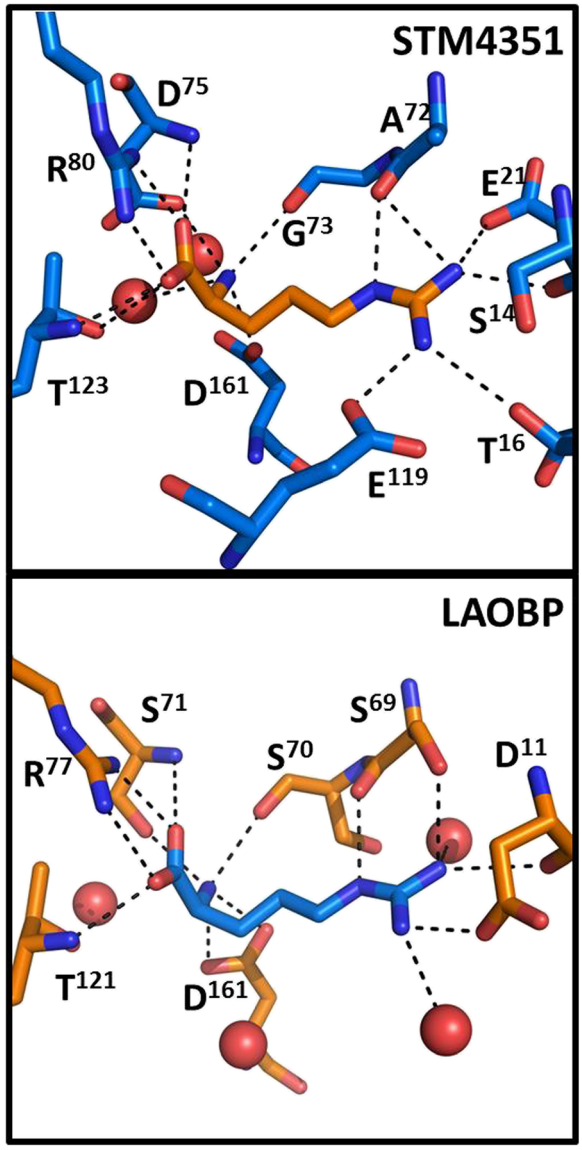

Figure 5. Schematic representation of the binding sites of STM4351 and LAOBP bound to Arg (PDB codes 2YTI and 1LAF, respectively). Only residues forming hydrogen bonds with the ligand are shown. Crystallographic water molecules are shown as spheres.

The disparate energetic strategies that PBPs have evolved for ligand recognition are not only determined by the different chemical nature of their ligands. In this regard, it is interesting to contrast the behaviors of LAOBP and STM4351. These *Salmonella* PBPs bind to Arg with quite dissimilar strength. At room temperature, the affinity of STM4351 for Arg is nearly 5 kcal mol^{-1} lower than that of LAOBP (Stamp *et al*., 2011). In spite of the low sequence identity (~33%), the two proteins preserve basically the same overall binding-site architecture, forming the same set of hydrogen bonds with Arg (Figure 5). The main difference between the two binding sites lies in the residues that interact with the guanidinium group. The aforementioned bidentate interaction of Asp^{11} in the LAOBP–Arg complex is not observed in the STM4351 complex; in the latter case, this interaction is replaced by the interaction with Ser^{14} and Thr^{16}. Besides, the hydrogen bonds formed by two structural water molecules in LAOBP are replaced by interactions with residues Glu^{21} and Glu^{119} in STM4351. Intriguingly, in spite of these rather small structural differences, LAOBP binding is enthalpy driven and STM4351 binding is entropy driven. These opposing behaviors may therefore be related to differences in the strength or cooperativity of protein–ligand interactions or to other aspects of the binding event, such as the dynamics and energetics of the "Venus flytrap" conformational change (Stamp *et al*., 2011).

In conclusion, the ligand-binding thermodynamic signatures in the PBP family are very diverse; millimolar to picomolar affinities can be driven by enthalpy and/or entropy changes. In the case of LAOBP, nanomolar affinity is achieved by enthalpy optimization.

Acknowledgements

N.O.P. is a recipient of a postdoctoral fellowship from Dirección General de Apoyos al Personal Académico (DGAPA)—Universidad Nacional Autónoma de México. The authors acknowledge the technical assistance from Dr. Isabel Velázquez-López and Dr. Laura Álvarez Añorve.

Grant sponsor, Consejo Nacional de Ciencia y Tecnología; grant number, 99857, 129239, and 167838; grant sponsors, DGAPA, Programa de Apoyo a Proyectos de Investigación e Innovación Tecnológica; grant numbers, IN205712, IN206510, IN215612, and IN219913.

REFERENCES

Abbott DW, Boraston AB. 2007. Specific recognition of saturated and 4,5-unsaturated hexuronate sugars by a periplasmic binding protein involved in pectin catabolism. *J. Mol. Biol.* **369**: 759–770.

Ames GFL. 1986. Bacterial Periplasmic Transport Systems: Structure, Mechanism and Evolution. *Ann. Rev. Biochem.* **55**: 397–425.

Aryal BP, Brugarolas P, He C. 2012. Binding of ReO_4^- with an engineered MoO_4^{2-} binding protein: towards a new approach in radiopharmaceutical applications. *J. Biol. Inorg. Chem.* **17**: 97–106.

Baker BM, Murphy KP. 1998. Prediction of binding energetics from structure using empirical parameterization. *Methods Enzymol.* **295**: 294–315.

Bello M, Pérez-Hernández G, Fernández-Velasco DA, Arreguín-Espinosa R, García-Hernández E. 2008. Energetics of protein homodimerization: effects of water sequestering on the formation of β-lactoglobulin dimer. *Proteins: Struct. Funct. Bioinf.* **70**: 1475–1487.

Berntsson RPA, Smits SHJ, Schmitt L, Slotboom DJ, Poolman B. 2010. A structural classification of substrate-binding proteins. *FEBS Lett.* **584**: 2605–2617.

Bevers LE, Hagedoorn PL, Krijger GC, Hagen WR. 2006. Tungsten transport protein A (WtpA) in *Pyrococcus furiosus*: the first member of a new class of tungstate and molybdate transporters. *J. Bacteriol.* **188**: 6498–6505.

Cadieux N, Bradveer C, Reeger-Schneider E, Köster W, Mohanty AK, Wiener MC, Kadner RJ. 2002. Identification of the Periplasmic Cobalamin-Binding Protein BtuF of *Escherichia coli*. *J. Bacteriol.* **184**:706–717.

Chavelas EA, García-Hernández E. 2009. Heat capacity changes in carbohydrates and protein-carbohydrate complexes. *Biochem. J.* **420**: 239–247.

Chu BCH, Chan DI, DeWolf T, Periole X, Vogel HJ. 2014. Molecular dynamics simulations reveal that apo-HisJ can sample a closed conformation. *Proteins* **82**: 386–398.

Cooper A. 2005. Heat capacity effects in protein folding and ligand binding: a re-evaluation of the role of water in biomolecular thermodynamics. *Biophys. Chem.* **115**: 89–97.

Davies GT, Hubbard ER, Tame HRJ. 1999. Relating structure to thermodynamics: The crystal structures and binding affinity of eight OppA-peptide complexes. *Protein Sci.* **8**: 1432–1444.

De Wolf FA, Brett GM. 2000. Ligand-Binding Proteins: Their Potential for Application in Systems for Controlled Delivery and Uptake of Ligands. *Pharmacol. Rev.* **52**: 207–236.

Doig AJ, Sternberg MJE. 1995. Side-chain conformational entropy in protein folding. *Protein Sci.* **4**: 2247–2251.

Dwyer MA, Hellinga HW. 2004. Periplasmic binding proteins: a versatile superfamily for protein engineering. *Curr. Opin. Struct. Biol.* **14**: 495–504.

Felder CB, Graul RC, Lee YA, Merkle HP, Sadee W. 1999. The Venus Flytrap of Periplasmic Binding Proteins: An Ancient Protein Module Present in Multiple Drug Receptors. *AAPS PharmSci* **1**: 1–20.

Fukada H, Sturtevant JM, Quiocho FA. 1983. Thermodynamics of the Binding of L-Arabinose and of D-Galactose to the L-Arabinose-binding Protein of *Escherichia coli*. *J. Biol. Chem.* **258**: 13193–13198.

García-Hernández E, Zubillaga RA, Chavelas-Adame EA, Vázquez-Contreras E, Rojo-Domínguez A, Costas M. 2003. Structural energetics of protein-carbohydrate interactions: Insights derived from the study of lysozyme binding to its natural saccharide inhibitors. *Proc. Natl. Acad. Sci. U. S. A.* **12**: 135–142.

Goldberg RN, Kishore N, Lennen RM. 2002. Thermodynamic Quantities for the Ionization Reactions of Buffers. *J. Phys. Chem. Ref. Data* **31**: 231–370

Hu X, Zhao J, DeGrado WF, Binns AN. 2013. *Agrobacterium tumefaciens* recognizes its host environment using ChvE to bind diverse plant sugars as virulence signals. *Proc. Natl. Acad. Sci. U. S. A.* **110**: 678–683.

Jeffery CJ. 2011. Engineering periplasmic ligand binding proteins as glucose nanosensors. *Nano Rev.* **2**: 5743–5746.

Lazaridis T, Archontis G, Karplus M. 1995. Enthalpic contribution to protein stability: Insights from atom-based calculations and statistical mechanics. *Adv. Protein Chem.* **47**: 231–306.

Makhatadze GI, Privalov PL. 1990. Heat Capacity of proteins. I Partial molar heat capacity of individual amino acid residues in aqueous solution Hydration effect. *J. Mol. Biol.* **213**: 375–384.

Makhatadze GI, Privalov PL. 1993a. Contribution of Hydration to Protein Folding Thermodynamics. II The Entropy and Gibbs Energy of Hydration. *J. Mol. Biol.* **232**: 639–659.

Makhatadze GI, Privalov PL. 1993b. Contribution of Hydration to Protein Folding Thermodynamics. I The Enthalpy of Hydration. *J. Mol. Biol.* **232**: 660–679.

Makhatadze GI, Privalov PL. 1995. Energetics of protein structure. *Adv. Protein Chem.* **47**: 307–425.

Mattle D, Zeltina A, Woo JS, Goetz BA, Locher KP. 2010. Two stacked heme molecules in the binding pocket of the periplasmic heme-binding protein HmuT from *Yersinia pestis*. *J. Mol. Biol.* **404**: 220–231.

Murphy KP, Freire E. 1992. Thermodynamics of structural stability and cooperative folding behavior in proteins. *Adv. Protein Chem.* **43**: 313–361.

Myers JK, Pace CN, Scholtz JM. 1995. Denaturant m values and heat capacity changes: relation to changes in accessible surface areas of protein unfolding. *Protein Sci.* **4**: 2138–2148.

Nikaido K, Ames GFL. 1992. Purification and Characterization of the Periplasmic Lysine, Arginine-, Ornithine- binding Protein (LAO) from *Salmonella typhimurium*. *J. Biol. Chem.* **267**: 20706–20712.

Oh BH, Pandit J, Kang CH, Nikaido K, Gokcen S, Ames GFL, Kim SH. 1993. Three-dimensional Structures of the Periplasmic Lysine/Arginine/Ornithine- binding protein with and without ligand. *J. Biol. Chem.* **268**: 11348–11355.

Oh BH, Ames GFL, Kim S. 1994. Structural Basis for Multiple Ligand Specificity of the Periplasmic Lysine-, Arginine-, Ornithine- binding Protein. *J. Biol. Chem.* **269**: 26323–26330.

Ortega G, Castaño D, Diercks T, Millet, O. 2012. Carhohydrate Affinity for the Glucos-Galactose Binding Protein Is Regulated by Allosteric Domain Motions. *J. Am. Chem. Soc.* **134**: 19869–19876.

Parsegian VA, Rand RP, Rau DC. 1995. Macromolecules and water: probing with osmotic stress. *Methods Enzymol.* **259**: 43–94.

Prabhu NV, Sharp KA. 2005. Heat capacity in proteins. *Annu. Rev. Phys. Chem.* **56**: 521–548.

Prajapati RS, Indu S, Varadarajan R. 2007. Identification and Thermodynamic Characterization of Molten Globule States of Periplasmic Binding Proteins. *Biochemistry* **46**: 10339–10352.

Pulido NO, Chavelas EA, Turner F, García-Hernández E. 2008. Current applications of isothermal titration calorimetry to the study of protein complexes. Advances in Protein Physical Chemistry, García-Hernández E, Fernández-Velasco DA (eds). Transworld Research Network: India; 115–138.

Quiocho FA. 1990. Atomic structures of periplasmic binding proteins and the high-affinity active transport systems in bacteria. *Phil. Trans. R. Soc. Lond. B* **326**: 341–351.

Record MT, Zhang W, Anderson CF. 1998. Analysis of effects of salts and uncharged solutes on protein and nucleic acid equilibria and processes: a practical guide to recognizing and interpreting polyelectrolyte effects, Hofmeister effects, and osmotic effects of salts. *Adv. Protein Chem.* **51**: 281–353.

Rose GD, Wolfenden R. 1993. Hydrogen Bonding, Hydrophobicity, packing and protein folding. *Annu. Rev. Biophys. Biomol. Struct.* **22**: 381–415.

Salmon RC, Cliff MJ, Rafferty JB, Kelly DJ. 2013. The CouPSTU and TarPQM Transporters in *Rhodopseudomonas palustris*: Redundant, Promiscuous Uptake Systems for Lignin-Derived Aromatic Substrates. *PLoS One* **8**: e59844.

Scheib U, Shanmugaratnam S, Farías-Rico JA, Höcker B. 2014. Change in protein-ligand specificity through binding pocket grafting. *J. Struct. Biol.* **185**: 186–192.

Schreier B, Stumpp C, Wiesner S, Höcker B. 2009. Computational design of ligand binding is not a solved problem. *Proc. Natl. Acad. Sci. U. S. A.* **106**: 18491–18496.

Silva DA, Domínguez-Ramírez L, Rojo-Domínguez A, Sosa-Peinado A. 2011. Conformational dynamics of L-lysine, L-arginine, L-ornithine binding protein reveals ligand-dependent plasticity. *Proteins* **79**: 2097–2108.

Sleigh SH, Seavers PR, Wilkinson AJ, Ladbury JE, Tame JRH. 1999. Crystallographic and Calorimetric Analysis of Peptide Binding to OppA Protein. *J. Mol. Biol.* **291**: 393–415.

Spolar RS, Livingstone JR, Record MT, Jr. 1992. Use of liquid hydrocarbon and amide transfer data to estimate contributions to thermo- dynamic functions of protein folding from the removal of nonpolar and polar surface from water. *Biochemistry* **31**: 3947–3955.

Stamp AL, Owen P, El KO, Lockyer M, Lamb HK, Charles IG, Hawkins AR, Stammers DK. 2011. Crystallographic and microcalorimetric analyses reveal the structural basis for high arginine specificity in the *Salmonella* enteric *serovar Typhimurium* periplasmic binding protein STM4351. *Proteins* **79**: 2352–2357.

Sturtevant JM. 1977 Heat capacity and entropy changes in processes involving proteins. *Proc. Natl. Acad. Sci. U. S. A.* **74**: 2236–2240.

Thomson J, Liu Y, Sturtevant JM, Quiocho FA. 1998. A thermodynamic study of the binding of linear and cyclic oligosaccharides to the maltodextrin-binding protein of *Escherichia coli*. *Biophys. Chem.* **70**: 101–108.

Velázquez-Campoy A, Freire E. 2006. Isothermal titration calorimetry to determine association constants for high-affinity ligands. *Nat. Protoc.* **1**: 186–191.

Vercillo NC, Herald KJ, Fox JM, Der BS, Dattelbaum JD. 2007. Analysis of ligand binding to a ribose biosensor using site-direct mutagenesis and fluorescence spectroscopy. *Protein Sci.* **16**: 362–368.

Whiteside GM, Krishnamurthy VM. 2005. Designing ligands to bind proteins. *Q. Rev. Biophys.* **38**: 385–395.

Wiseman T, Williston S, Brandts JF, Lin LN. 1989. Rapid measurement of binding constants and heats of binding using a new titration calorimeter. *Anal. Biochem.* **179**: 131–137.

Zakariassen H, Sørlie M. 2007. Heat capacity changes in heme protein-ligand interactions. *Thermochim. Acta* **464**: 24–28.

Zakariassen H, Cederkvist FH, Harbitz E, Shimizu T, Lange R, Mayer B, Gorren ACF, Andersson K, Sorlie M. 2008. Thermodynamic analysis of L-arginine and N^{ω} -hydroxy-L-arginine binding to nitric oxide synthase. *Biochim. Biophys. Acta* **1784**: 806–810.

Zhang H, Herman PJ, Bolton H, Jr., Zhang ZA, Clark S, Xun L. 2007. Evidence that Bacterial ABC-Type Transport Imports Free EDTA for Metabolism. *J. Bacteriol.* **189**: 7991–7997.

SUPPORTING INFORMATION

Additional supporting information may be found in the online version of this article at the publisher's web site.

